Universiteit Leiden

The Netherlands

Absorption, luminescence and scattering of single nano-objects
Yorulmaz, M.

Citation
Yorulmaz, M. (2013, June 26). *Absorption, luminescence and scattering of single nano-objects*. *Casimir PhD Series*. Retrieved from https://hdl.handle.net/1887/21018

Cover Page

Universiteit Leiden

Author: Yorulmaz, Mustafa
Title: Absorption, luminescence, and scattering of single nano-objects
Issue Date: 2013-06-26

Absorption, luminescence and sizing of organic dye nanoparticles

Organic nanoparticles made of a push-pull triarylamine dye with an average diameter of 60 nm, were prepared by reprecipitation. We study their photophysical properties by a combination of photothermal and fluorescence microscopy. Photothermal contrast provides a quantitative measure of the number of absorbers. The size of nanoparticles estimated from the absorption measurements was compared with sizes measured by AFM. Fluorescence and absorption microscopy provide quantum yield on the single-particle level as a function of excitation intensity. The quantum yield strongly decreases at high intensities because of singlet-singlet or singlet-triplet annihilation. We also report the formation of molecular thin layers and of labyrinthshaped structures on glass substrates, presumably induced by dewetting.

3.1 Introduction

For decades, nanoparticles that are composed of metal and inorganic semi-conductor materials have attracted much attention due to their unique size-dependent optical properties.[71,133–135] Various organic molecules with large structural diversity can form nanometer-sized particles (10-250 nm diameter). These nanoparticles are typically prepared by reprecipitation,[54] sol-gel formation,[136] laser fabrication,[137] or reprecipitation-encapsulation.[138] Organic nanoparticles are potential labels for biomedical imaging and sensing,[139–141] as well as promising materials for the fabrication of organic light-emitting diodes, field-effect and thin-film transistors, and photovoltaic solar energy collectors.[1,2] Self-organized patterns of nanoparticles[66,142] have been credited for the tunability of charge transport[143] and optical properties.[144] Strong correlations between morphology and fluorescence properties were demonstrated by near-field scanning optical microscopy in thin films of organic materials.[145,146] Considerable attention is currently paid to multicolor emission of organic nanoparticles under monochromatic excitation, and to the control of the emission range by changing only one active unit of a dye.[147] Also, Gesquiere et al. have shown that the emission color depends on the crystal structure of perylene-derivative nanoparticles, which is related to the size of nanoparticles.[43] For conjugated polymers, Wang et al. observed an increase in the fluorescence intensity with the size of alkyl-PTA and alkoxy-PTA nanoparticles (smallest size of 100 nm), and changes in the absorption spectrum upon their aggregation-driven growth.[148]

Light-scattering, absorption and fluorescence microscopy are typically used for investigating ensembles of organic nanoparticles. For individual nanoparticles, however, most scattering methods work well only for particles with diameters larger than 40 nm,[42,149,150] and a few are capable to visualize smaller diameters.[86–88] Alternatively, detection of individual gold nanoparticles with diameter down to 1.4 nm,[42,93] and even single organic molecules at room temperature are demonstrated in absorption microscopy.[82,91,92,104] Well-established fluorescence microscopy provides a broad range of methods that are used in biology, chemistry and material science.[36,151–154] A combination of photothermal microscopy and fluorescence microscopy[155,156] provides simultaneous insight into the absorption and fluorescence characteristics of single nanoparticles.

Here, we have selected 4-di(4′-*tert*-butylbiphenyl-4-yl)amino-4′-dicyanovinylbenzene (fvin)[147] molecule because of its absorption maximum around 450 nm, near the monochromatic excitation wavelength (514 nm), and for its red-shifted emission, peaking at around 620 nm, provided by a strongly distorted charge-transfer excited state. Along with its emission properties, the fvin excited state exhibits significant radiationless deactivation to the ground state through efficient vibrational processes. The heat dissipated upon internal conversion is detected in photothermal microscopy as a refractive index change of the local environment. Moreover, the peripheral bulky groups prevent the molecules from forming dark $\pi - \pi$ adducts. Finally, the complex shape and flexible backbone of fvin enables the formation of stable spherical fvin nanoparticles, giving rise to colloidal solutions by means of a simple reprecipitation method without the use of any surfactant.

In addition to previously stated optical and physical properties of fvin that make its NPs a suitable candidate for combined photothermal and fluorescence microscopy experiments, we find that microstructures are formed upon dewetting of the precipitate suspension. Similar structures are believed to favor charge collection in solar cells.[157]

Herein, photothermal[82] microscopy and fluorescence microscopy are first simultaneously applied for quantitative characterization of single immobilized organic nanoparticles (NPs) formed from the fvin molecule.[147] Then, the same characterization is employed on the dewetting induced microstructures. The combined technique reveals the complex luminescence mechanism affected by singlet-singlet or singlet-triplet annihilation and is utilized to determine the luminescence quantum yield of each individual fvin NP. The number of molecules in each individual NP is obtained from their absorption signal, luminescence signal and their volume. The number of molecules building up the structures is deduced from their optical absorption.

3.2 Experimental section

3.2.1 Combined photothermal and fluorescence microscopy

Optical microscopy experiments were performed on a combined photothermal and fluorescence microscope, home-built around an inverted optical

microscope (Olympus IX-71). The optical setup is schematically shown in Fig. 3.1. Details of photothermal detection were described in Chapter 2. In addition, the 514 nm emission of an Ar-ion laser (Coherent Inc, Innova 310, 10 W) was used here for both fluorescence excitation and photothermal heating of nanoparticles to detect them simultaneously in fluorescence and absorption, respectively. The same laser pumped a tunable continuous wave Ti:Sapphire laser (Spectra Physics, S3900s) which operated at 800 nm and served as a probe laser for absorption measurements.

For photothermal imaging, the intensity of the heating beam was modulated ($\sim$1 MHz) using an acousto-optic modulator (AOM, AA Optoelectronic) or an acousto-optical tunable filter (AOTF, AA Optoelectronic). In the latter case, the AOTF was also used to select the desired emission line from the Ar-Ion laser. The heating and the probe beams were expanded ($\sim$20 mm) and spatially overlapped on a dichroic mirror (BS 669, AHF or 595 DCXRR, AHF) by means of telescopes. Two different telescopes were used for heating and the probe beams to adjust their overlap in the focus of the oil immersion microscope objective (Olympus, 60$\times$, NA=1.45), thereby compensating for chromatic aberrations. Both beams were focused on the sample using the microscope objective (Olympus, 60X oil immersion, numerical aperture 1.45) after being reflected by a dichroic mirror (AHF z532/NIR). Nanoparticles were deposited on a cover glass and immersed in glycerol.

The back-reflected probe beam and fluorescence signals were collected by the same microscope objective and sent towards the dichroic mirror (AHF z532/NIR), which was separating the heating and probe light from the fluorescence signal. The probe beam passed through a 50/50 beamsplitter, longwave pass filters (LWP700, LWP750), and was focused on a variable-gain Si photodiode (Femto DHPCA-100-F). The output of detected signal was fed into a lock-in amplifier (SR844, Stanford Research Systems) and the photothermal signal was obtained by isolating the small modulated component from the high DC signal arising from the reflection of the probe beam from the glass-glycerol interface.

For luminescence imaging, the luminescence signal of nanoparticles, which was obtained by excitation at 514 nm, was spatially filtered by a 30 μm confocal pinhole and spectrally selected by a set of bandpass filters (AHF 615/150 and Omega 590/100), and was focused on a single-photon-counting avalanche photodetector (SPCM-AQR-16, Perkin-Elmer).

The experiment was controlled by using a home-written LabVIEW software. Data were collected by a data acquisition card (ADWin Gold, Germany). The raster-scan imaging was provided by a three-axis piezostage (Mars II, Physik Instrumente). ImageJ was used for data analysis.
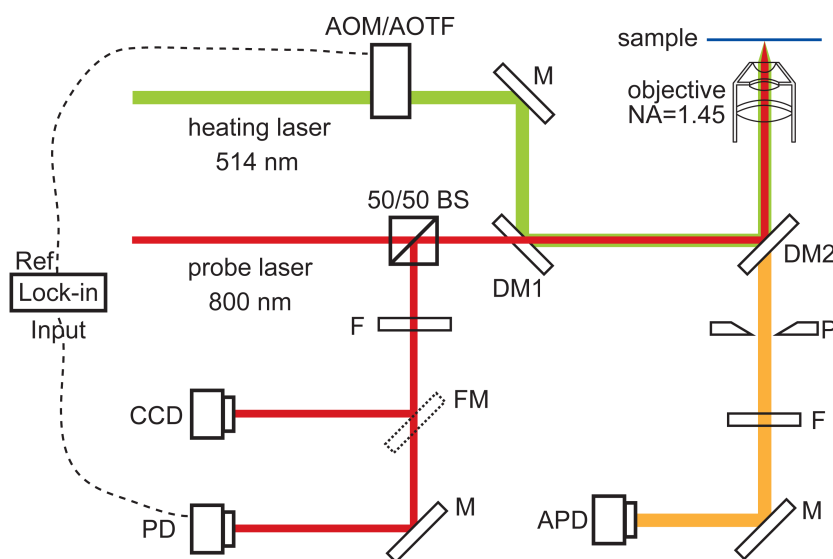
Figure 3.1: Schematic of the experimental setup for simultaneous absorption and luminescence detection. AOM - acousto-optic modulator, AOTF - acousto-optical tunable filter, M - mirrors, FM - flip mirror, DM - dichroic mirrors, F - filter, PD - photodiode, CCD - video camera, APD - avalanche photodetector. Beam expanding telescopes, focusing lenses, polarizers and spatial filters are not shown in this scheme.

3.2.2 Atomic force microscopy

Height distributions of organic nanoparticles were characterized with AFM (Veeco/Digital Instruments, Nanoscope IIIa) equipped with 280 kHz or 70 kHz resonance frequency commercial cantilevers working in tapping mode in air. (see Appendix B, Fig. B.1 for AFM image and height distributions)

3.2.3   Organic nanoparticles preparation

A push-pull triarylamine dye (fvin),[147] insoluble in water, was used for the preparation of the stock solution at a weight percentage ranging within 0.01-1 wt% in acetone. Nanoparticles were formed through reprecipitation of the compound upon addition of the stock solution in Milli-Q water (Millipore Corp.). A volume of 50 μL or 100 μL (giving similar results) of a stock fvin solution was quickly injected into vigorously stirred Milli-Q water (5 mL) (see Appendix B, Fig. B.2 for chemical structure and bulk spectroscopy results).

3.2.4   Sample preparation for optical microscopy

Glass coverslips (Menzel, Germany) were cleaned in the same way as in Section 2.4.1. Clean coverslides were functionalized with 3-aminopropyl triethoxy silane (APTES, Sigma-Aldrich) to facilitate the adhesion of fvin NPs to glass from water solution. Silanization was performed in liquid phase by immersing clean glass slides overnight in a 2% solution of APTES in spectroscopic-grade acetone. The slides were then sonicated in acetone and water, dried and shortly stored prior to use.

Nanoparticles were deposited on these surfaces by one of the following methods: 1) through incubation of 50 μL of NPs solution for 1-20 s on silanized coverslides, followed by gentle washing with 5-7 mL of Milli-Q water. Attention was paid to prevent dewetting of the sample by keeping it immersed in each step of NP deposition. This preparation method is used to prevent sublimation of fvin NPs in dry conditions; 2) through incubation of 50 μL of NPs solution for 1-2 hr, followed by an exchange of solution with pure water or glycerol; or 3) through spin-coating of 50 μL of nanoparticles solution in a 1% PVA matrix at 2000 rpm for 5 s, followed by drying at 4000 rpm for 90 s. The last two options involve dewetting of the sample and can induce pattern formation (see Section 3.3.2).

Optical experiments were performed in a fluid cell with a volume of approximately $50 - 150$ μL filled with glycerol ($> 99.5\%$, spectrophotometric grade).

3.3 Result and discussion

3.3.1 Optical microscopy of organic nanoparticles

We performed photothermal and fluorescence microscopy experiments on individual fvin NPs, which were formed through reprecipitation in water of fvin stock solutions at three concentrations (0.1, 0.5 and 1 wt%) in acetone. Experiments were carried out in two regimes for the heating/excitation power at the sample: low (0.85-1.7 μW), and high (8.5-130 μW) (see Appendix B, Fig. B.3, B.4). While simultaneous photothermal and fluorescence detection of NPs was possible at the high heating power regime, only a few NPs provided detectable photothermal signal at low heating regime. Therefore, most of the fluorescence raster scans at low heating power were accompanied by raster scans where fluorescence and photothermal were simultaneously recorded at high heating power. The photothermal signals acquired at high heating power were then used as a measurement of the NP absorption at low heating power. We were not able to increase the probe power to gain more sensitivity in photothermal detection[90] since we observed a weak two-photon excited fluorescence emission for probe powers higher than 50 mW at the sample. No two-photon excited fluorescence was detected with probe powers up to 40 mW.

Typical photothermal and fluorescence images of nanoparticles deposited in solution on an APTES-modified glass in glycerol, which are simultaneously acquired at high heating power regime, are shown in Fig. 3.2 A and 3.2 B, respectively. Spatially separated spots with different signal strengths, which correspond to individual nanoparticles, are observed in both images. About 1% of spots in raster scans are only visible in photothermal but not in fluorescence images (dashed circle), or in fluorescence but not in photothermal images (dashed box). The absence of fluorescence in some NPs can be explained by the presence of quenching states, originating, for example, from a small concentration of impurities in the solvents or the embedding liquids. The absence of photothermal signal of some fluorescent NPs points to a small number of fvin molecules, or to a fluorescent impurity with a high quantum yield. A different packing of fvin molecules may also lead to higher fluorescence due to inhibition of the radiationless deactivation. The large spread of magnitudes of both signals suggests that nanoparticles have a wide dis-

tribution of sizes, that is, of numbers of fvin molecules. Further analysis of optical signals from NPs was performed on selected spots with a photothermal signal-to-noise ratio (SNR) larger than 5.

The correlation between the fluorescence signal and the photothermal signal for the same individual fvin NPs, first in the low and then in the high excitation power regimes is shown in Fig. 3.2 C. The normalized photothermal signal reveals up to 10 times smaller absorption compared with 20 nm diameter gold nanoparticles (AuNPs) that were used as fiducial markers.
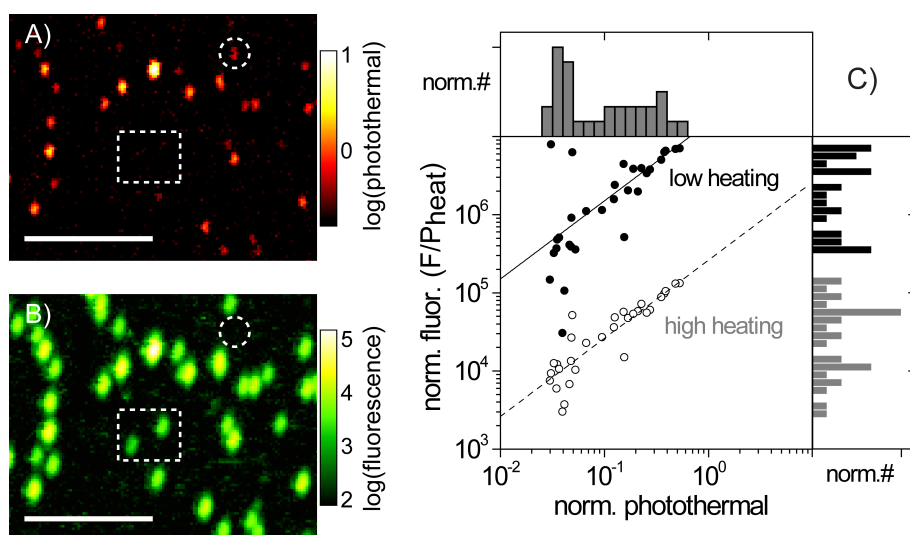

Figure 3.2: Simultaneous A) photothermal and B) fluorescence images of 0.5 wt% fvin NPs deposited on APTES-modified glass in glycerol. The scale bar is 5 μm. A dashed circle highlights a spot observed in the photothermal, but not in the fluorescence image, while a dashed box indicates two fluorescent spots that are not detectable in the photothermal image. The pump power used in the experiment is 106 μW, the probe power is 34 mW. The acquisition time per pixel is 10 ms with 3 ms lock-in integration time for photothermal signal. C) Correlation of normalized fluorescence with photothermal signals consequently measured on the same fvin NPs in two excitation regimes. The fluorescence intensity is in units of 100 counts s^{-1} mW^{-1}. Solid and dashed lines represent linear relationship between signals

Firstly, we observe a rough linear relationship between normalized photothermal and fluorescence signals in both regimes. We conclude that the fluorescence signal scales roughly linearly with the volume of NPs, since we

expect the photothermal signal to be proportional to the number of absorbing molecules, which scales as the NP volume. Indeed, direct correlations of AFM and optical microscopy images would reveal the relationship between a NP's size and its optical signals, similar to studies on individual spherical gold NPs.[156] We tried to obtain such correlations. However, it turned out to be difficult due to sublimation of fvin NPs in air. Secondly, the fluorescence intensity normalized to the excitation power decreases strongly with the excitation intensity (see Appendix B, Fig. B.5). We attribute this decrease of the fluorescence quantum yield to singlet-singlet or singlet-triplet annihilation, that is, to quenching of fvin excited state by other excited states in its surroundings. This phenomenon is well-known in other multichromophoric systems, such as conjugated polymers[158–161] and dendrimers.[162–166] Thirdly, we also note that photothermal and luminescence signals are better correlated at high power than at low power (see Appendix B, Fig.B.4). This observation is consistent with a quenching effect dominated at high power by singlet-singlet annihilation, a bulk effect. At low power, however, we expect quenching to occur mainly through surface and trap effects.

The complex behavior of absorption and fluorescence properties of fvin NPs is further complicated by photobleaching. Fluorescence and photothermal signals bleach upon exposure to the excitation power of 8.5 μW with characteristic times of 0.81 s and 0.84 s, respectively (Fig. 3.3). We find that the bleaching rates do not depend on the initial signal from individual NPs (or nanoparticle sizes), and rise as the heating power increases. At an excitation power of 17 μW, the fluorescence intensity is reduced by a factor of three after a dwell time of about 100 ms. There is negligible bleaching from exposure to probe powers less than 40 mW. In order to minimize the effect of bleaching at a given heating power, we shortened the exposure times in a raster scan to 10 ms per pixel (we had up to 25 pixels per NP in a two-dimensional raster scan).

Then, we calculate the average luminescence quantum yield of fvin NPs in the low heating power regime using 20 nm gold nanoparticles (AuNPs) as fiducial markers for quantitative absorption measurements, and estimating the detection efficiency of the setup to 5%. The quantum yield we find, 0.017, measured on 83 fvin NPs, is in reasonable agreement with the values estimated for ensembles (i.e. 0.013 for suspension of fvin NPs of diameter 85 nm).[55] The apparent QY calculated for more than 1000 NPs in the high
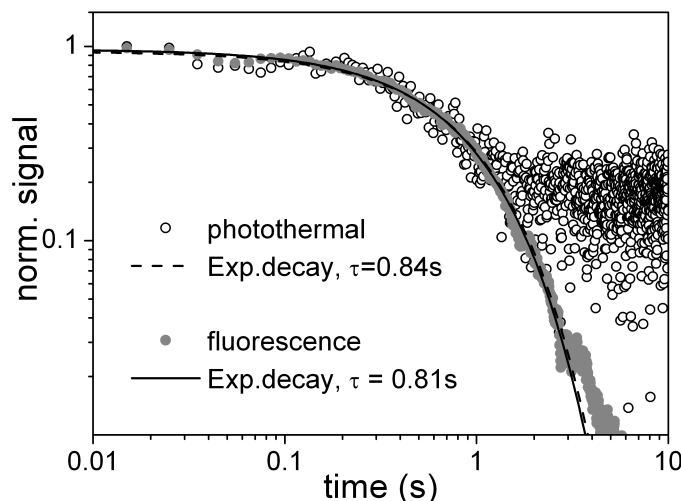
Figure 3.3: Photothermal (○) and fluorescence (●) signal bleaching traces measured on 0.1 wt% fvin NPs on APTES-modified glass in glycerol, shown on a log-log scale. Heating and probe powers were 8.5 μW and 23 mW, correspondingly. Characteristic bleaching times estimated from single exponential decay fits are 0.81 s, and 0.84 s for fluorescence (——) and photothermal (- - - -) signals, correspondingly. The normalized signal of about 0.2 is the background level of the photothermal signal.

heating power regime was found to be much lower, about 1.2×10^{-4} (see Appendix B, Fig. B.4).

Further, the number of molecules in individual fvin NPs is obtained in three different ways, from the photothermal signal, from the luminescence signal, and from the average height of NPs as measured by AFM (Appendix B, Table B.1):

1. The average absorption cross section of fvin NPs at 514 nm is about 180 nm^2. The average isotropic absorption cross section of an individual fvin dye molecule as deduced from the absorption spectrum of fvin NPs in glycerol is estimated to be about 3.2×10^{-3} nm^2 at 514 nm.[167,168] Thus, the average number of fvin molecules in an average fvin NP would be about 6×10^4.

2. We observe a fluorescence count rate of 600 kcounts s^{-1} under the excitation intensity of 1.7 kW cm^{-2} at 514 nm. Assuming a quantum yield of 10^{-2} similar to that of the isolated molecule, we deduce an absorption rate for an individual fvin NP of 1.2×10^9 photons s^{-1}. From

the number of photons absorbed by a single fvin dye molecule, about 1.4×10^5 photons s^{-1}, calculated from the absorption cross section at the same intensity, there would be $\sim 10^4$ molecules on average in a particle.

3. AFM measurements (Appendix B, Fig. B.1) give an average volume of 4×10^5 nm^3 for the NPs, assumed to be spherical.[55] The molecular Van der Waals volume of fvin is 0.85 nm^3. If the molecules are compactly packed in the NP, about 5×10^5 molecules would be present in a single fvin NP.

These independent estimates of about $10^4 - 10^5$ molecules per fvin NP are in reasonable agreement for these three independent methods.

3.3.2 Submonolayers and labyrinth structures formed by organic molecules

Figure 3.4 shows photothermal and fluorescence microscopy images of fvin NPs prepared from 0.025 wt% (Fig. 3.4 A-D) and 0.013 wt% (Fig. 3.4 E) solutions. We observe weak signals from surface structures besides intense spots of individual NPs. For instance, a net-shaped pattern is visible both in photothermal and fluorescence images (Fig. 3.4 A,B). The average photothermal and fluorescence signals of the net-shaped pattern are about 30 times and 500 times smaller than the average of 15 individual NPs in Fig. 3.4 A and 3.4 B, respectively. The characteristic size of meshes is about 5 μm. In some regions we further observe brighter structures like the ones shown in Fig. 3.4 C,D on the right side. The photothermal and fluorescence signals of these structures are about 5 times and 10 times higher than of the net-shaped patterns in the same images, respectively.

Formation of similar patterns via self-organization of molecules/nanoparticles from solution during dewetting has been reported in the literature.[62–64,169–173] Their origin is generally explained by instabilities driven by intermolecular and surface forces at solid-liquid-air interfaces, which are influenced by the solvent, the concentration of nanoparticles, the deposition method, the substrate and the temperature. We attribute the observed morphologies to such instabilities occurring during sample preparation either during the drying step of the spin-coating, or during the sample washing steps. In addition, samples obtained from
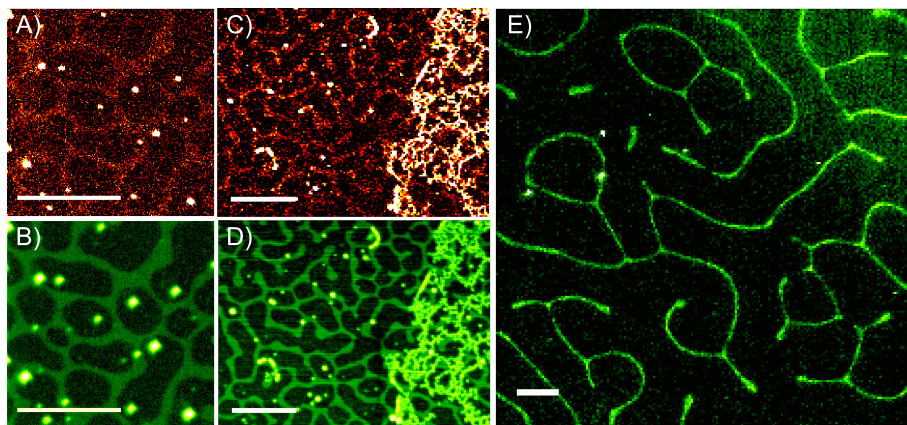
Figure 3.4: Photothermal (A,C) and corresponding simultaneously acquired fluorescence images (B,D) of net-shaped patterns formed on glass from 0.025 wt% fvin NPs in water. The pump power used in the experiment is 43 μW, the probe power is 23 mW. The acquisition time per pixel is 10 ms with 3 ms lock-in integration time for photothermal signal. E) Fluorescence image of a labyrinth pattern formed from 0.013 wt% fvin NPs in 1% PVA/water solution deposited on clean glass through spin-coating. The average fluorescence signal of bright labyrinth walls is 120 kcounts per 10 ms with the SNR of 5. The heating power is 260 μW, the probe power is 23 mW. The acquisition time per pixel is 10 ms. The photothermal signal is not detectable at these experimental conditions. The average spacing between the ridges in the fluorescence image in (E) is about 12 μm. The white scalebar for all images is 10 μm.

low-concentration NP solutions are expected to yield less dense structures in surface-tension-driven dewetting processes.[62] This explanation is supported by the observation of a labyrinth-like pattern with bright fluorescent ridges and the average spacing of about 12 μm (Fig. 3.4 E). These patterns were obtained by spin-coating a suspension obtained by diluting the original suspension of fvin NPs —water precipitated from 0.013 wt percent stock dye solution in acetone— into a 1 wt% solution of PVA in water. This image further resembles the labyrinth patterns formed in confined granular-fluid systems due to instabilities at the fluid-air interface, as described by Sandnes et al.[170] These authors report a notable decrease of the average spacing in the pattern and a slight thickening of ridges with increasing volume fraction of the grains. The features we observe are similar to those, but their characteristic length scale is four orders of magnitude smaller. It will be interesting to investigate whether the physical mechanisms behind pattern

formation are the same on those very different spatial scales.

It would be natural to assume that the structures in Fig. 3.4 A-D, displaying the same brightness everywhere, are formed by one monolayer of the dye. Let us estimate the number of molecules in the net-shaped patterns, assuming those are formed by fvin molecules that give rise to photothermal and fluorescence signals. If all molecules in the laser spot would be concentrated in a nanoparticle, the quantitative photothermal measurement would give an absorption cross section of $0.5 - 3.2$ nm^2. This corresponds to 150-1000 molecules, based on the absorption cross section of an individual molecule, 3.2×10^{-3} nm^2 (Appendix B, Table B.1). This number is about two to three orders of magnitude smaller than the expected number of fvin molecules packed in this area in a monolayer. Although the spread of the absorbing molecules over the whole laser spot may weaken their photothermal signal, this density appears much lower than that of a packed monolayer.

The quantitative interpretation of the fluorescence images obtained in the high heating power regime is rather difficult due to the unknown morphology of the molecular organization of the pattern and to a combination of quenching and photobleaching. However, the luminescence count rate per molecule appears larger when molecules are compactly packed in a spherical fashion than when they are homogeneously distributed. Similar to the experiments with fvin NPs, both patterns and aggregates show degradation of photothermal and fluorescence signals with prolonged illumination or after performing several scans in the same sample area.

3.4 Conclusions

We have investigated the organic nanoparticles prepared by reprecipitation of a triarylamine dye, fvin. We have studied the optical absorption and emission properties of these spherical NPs by means of combined fluorescence and photothermal (absorption) microscopy at the single-particle level. We have found a roughly linear correlation of normalized fluorescence and photothermal signals at low and high excitation regimes. In the high heating power regime nanoparticles show an apparent fluorescence quantum yield 100 times lower than in the low heating power regime. We attribute this high-power quenching to singlet-singlet or singlet-triplet annihilation at the high concentration of excitations, presumably assisted by exciton migration. Sim-

ilar quenching effects are observed in many multichromophoric systems. We have calculated the (low-power) fluorescence quantum yield of individual fvin NPs to be about 10^{-2}, which is in good agreement with results obtained earlier on ensembles. Furthermore, we used photothermal microscopy, fluorescence microscopy and AFM for quantitative measurements of the average number of molecules in individual NPs. Results from these three independent methods reveal an average number of molecules per nanoparticle to be $10^4 - 10^5$. Finally, we report the formation of patterns with complex morphologies from fvin molecules and NPs, which are probably driven by dewetting upon sample preparation.

This work presents a first study of the optical properties of individual organic nanoparticles, which are different from conjugated polymers, inorganic, and metal nanoparticles. It illustrates the potential of correlated absorption and fluorescence studies for the investigation of such complex systems.

Acknowledgements